Applied Nanoscience (2018) 8:115–124
https://doi.org/10.1007/s13204-018-0654-7

ORIGINAL ARTICLE

Real-time cellular and molecular dynamics of bi-metallic self-therapeutic nanoparticle in cancer cells

Sandeep Kumar Vishwakarma[1,2] · Avinash Bardia[1,2] · Chandrakala Lakkireddy[1,2] · Syed Ameer Basha Paspala[1,2] · Md. Aejaz Habeeb[1,2] · Aleem Ahmed Khan[1,2]

Received: 16 September 2017 / Accepted: 18 November 2017 / Published online: 3 February 2018

Abstract

Since last decades various kinds of nanoparticles have been functionalized to improve their biomedical applications. However, the biological effect of un-modified/non-functionalized bi-metallic magnetic nanoparticles remains under investigated. Herein we demonstrate a multifaceted non-functionalized bi-metallic inorganic Gd-SPIO nanoparticle which passes dual high MRI contrast and can kill the cancer cells through several mechanisms. The results of the present study demonstrate that Gd-SPIO nanoparticles have potential to induce cancer cell death by production of reactive oxygen species and apoptotic events. Furthermore, Gd-SPIO nanoparticles also enhance the expression levels of miRNA-199a and miRNA-181a-7p which results in decreased levels of cancer markers such as C-met, TGF-β and hURP. One very interesting finding of this study reveals side scatter-based real-time analysis of nanoparticle uptake in cancer cells using flow cytometry analysis. In conclusion, this study paves a way for future investigation of un-modified inorganic nanoparticles to purport enhanced therapeutic effect in combination with potential anti-tumor drugs/molecules in cancer cells.

Keywords Gd-SPIO nanoparticles · MRI contrast · Cancer treatment · Real-time analysis

Introduction

Since last decades, major exploration of nanotechnology in biomedical applications has been extensively explored for imaging and cancer theranostics (Arvizo et al. 2012). Although cancer treatment strategies using functionalized nanoparticles have been significantly studied, the effect of un-modified bi-metallic nanoparticles remains under investigated (Arvizo et al. 2013). Nanoparticles have been considered as the most prominent vehicle for targeted drug-delivery in cancer cells due to their unique properties of passing the biological barriers and distribution within the cellular counterparts through receptor-mediated or energy-dependent pathways (Bhattacharya and Mukherjee 2008). Recent studies have explored several emerging nanoparticle-based potential modalities for drug delivery which implies the use of different cell machineries as targeted delivery system to release a therapeutic payload (Rengan et al. 2014, 2015; Krishnamurthy et al. 2016). The major focus of nano-drug delivery approaches has been on shape, size, functional moieties and nanoparticle interaction sites on cancer cells.

Although a variety of nanoparticle-based drug delivery carriers have been used successfully in pre-clinical settings, there remain a number of limitations for their real-time monitoring. In addition, the effect of non-functionalized bi-metallic nanoparticles on cancer cells needs to be investigated in more detail to improve better therapeutic response in cancer cells. Therapeutic or diagnostic molecules which are delivered in cancer cells through nanoparticles generally leak from the cells during the loading process and after certain time points released from the cells (Jiang et al. 2008). This may lead to decreased therapeutic response in cancer cells. Hence, development of a self-therapeutic nanoparticles and real-time monitoring of their delivery, bio-distribution, release and cellular response is of utmost important which can provide critical information required for dynamic

✉ Aleem Ahmed Khan
aleem_a_khan@rediffmail.com

[1] Central Laboratory for Stem Cell Research and Translational Medicine, Centre for Liver Research and Diagnostics (CLRD), Deccan College of Medical Sciences, Hyderabad, Telangana 500058, India

[2] Dr. Habeebullah Life Sciences, Attapur, Hyderabad, Telangana 500048, India

optimization of treatment modalities in more personalized manner in real-time.

The ability to monitor nanoparticle accumulation or release in target cancer cells and simultaneous investigation of the therapeutic response may enable an individualized feedback process to further adjust the treatment dose and protocols to meet the changing demands of each patient in more personalized manner. However, the lack of proper monitoring strategies for real-time assessment of cellular dynamics of nano-drug delivery and its consequential effects in cancer cells poses a potential challenge to develop more effective cancer treatment strategies. Earlier approaches are often carried out on end point analysis, rely on time-consuming bulk measurements and vary from one cell population to the other (Bridot et al. 2007; Mayhew et al. 2009; Benezra et al. 2011; Chan and Lin 2015). In addition, these strategies provide averaged results and do not guarantee for precise control over the nano-drug delivery to cancer cells. These approaches also do not generate sufficient useful informations for the dynamics of nanoparticle–cell or drug–cell interactions and/or nanoparticle-based drug delivery in cancer cells.

Hence, the current study was focused on real-time quantification and internalization of Gd-SPIO nanoparticles into cells using flow cytometry-based side-scatter approach. Dual-MRI contrast property of Gd-SPIO nanoparticles was also identified using 1.5T Magnetome to explore its potential in MRI-based cell tracking and tumor imaging. Furthermore, reactive oxygen species (ROS) generation, apoptosis and molecular analysis for oncogenic transcripts and miRNA expression were identified to better understand the cellular and molecular dynamics of bi-metallic nanoparticles loading in hepatoblastoma cells.

Materials and methods

All in vitro studies were conducted as per the guidelines of Institutional Review Board and animal studies were conducted after taking approval by the Institutional Animal Ethics Committee of Deccan College of Medical Sciences, Hyderabad.

Synthesis and characterization of Gd-SPIO nanoparticles

Gd-SPIO nanoparticles were synthesized using colloidal hydrolytic synthesis method as reported in our earlier study (Athar et al. 2016). Briefly, Gadolinium trichloride hexahydrate ($GdCl_3.6H_2O$) and anhydrous ferric trichloride ($FeCl_3$) were used as molecular precursors for synthesizing the nanoparticles. 12.31 mmol of $FeCl_3$ was stirred in deionized water for 6 h which was further mixed with similar concentration of $GdCl_3.6H_2O$ and refluxed additionally for 6 h. The reaction was cooled and filtered to remove the unreacted impurities. Following this calcination was performed at 10 °C/min from room temperature to 1000 °C. Further washing was performed to remove the ionic impurities. Synthesized Gd-SPIO bi-metallic nanoparticles were characterized extensively (Athar et al. 2016). In addition to basic chemical properties, nanoparticles were dissolved in acetonitrile and a UV–vis spectrum was identified using UV–Spectrophotometer (Perkin Elmer Lambda 35).

Scanning electron microscopy (SEM) studies

SEM images of Gd-SPIO nanoparticles were obtained using a Hitachi S520 Scanning Electron Microscope. Further, human liver cells were treated with these nanoparticles for 72 h and SEM analysis was carried out to identify the major changes in cell morphology and surface anatomy.

Biocompatibility studies

The biocompatibility of Gd-SPIO nanoparticles with human cells was identified using human liver cells which were incubated with different concentrations of Gd-SPIO nanoparticles ranging from 10 µg/ml to 1 mg/ml for 72 h in CO_2 incubator. The cell viability was determined by tetrazolium reduction assay. Briefly, cells were incubated with MTT reagent (2 mg/ml) in 96-well culture plates for 72 h. After incubation period, reaction was stopped using acidified isopropanol or acetone by additional incubation for 10 min. The optical density of samples was measured in triplicates in three individual experiments. However, the in vivo biocompatibility study was performed by infusing 200 µl of Gd-SPIO nanoparticles (1 mg/ml) into male Wister rats injected through tail vein. Histological analysis was performed for major vital organs using hematoxylin and eosine (H&E) staining to identify any abnormality in tissues. Other biocompatibility parameters and retention time of Gd-SPIO nanoparticles have been well demonstrated in our earlier study (Athar et al. 2016).

Magnetic resonance imaging (MRI)

The dual MRI-contrast property of Gd-SPIO nanoparticles was identified in vitro using 1.5T clinical Magnetome at Princess Esra Hospital, Hyderabad. 10, 100, 250, 500 µg/ml, 1 mg/ml concentrations of Gd-SPIO nanoparticles in water were kept in 12-well sterile cell culture plates at room temperature. MRI-contrast agents were categorized based on the changes in their relaxation times. The ratio of r2/r1 was identified to determine the T1 and T2 contrast properties of bi-metallic Gd-SPIO nanoparticles.

Side-scatter analysis (SCA)

To establish a real-time quantification for interaction between nanoparticles and cancer cells, human hepatoblastoma cell line (HepG2) was cultured in vitro and exposed to Gd-SPIO nanoparticles. Post-exposure of 10, 30, 60, 120 min, 24 and 48 h at 37 °C temperature and 5% CO_2 atmospheres, cells were harvested after completing each incubation time and subjected to flow cytometry-based side-scatter analysis (SCA). SCA was performed to determine the shift in cell scatter in flow cytometry post-nanoparticle exposure. Side scatter was extracted after flow cytometric measurements through gating of phenotypically healthy cells which was characterized by negative staining for Annexin-V (Sigma-Aldrich, St. Louis, MO, USA) and propidium iodide (Sigma-Aldrich, St. Louis, MO, USA). The values of each side scatter of untreated control cells were set to 100% and used for computing the relative increase in side scatter of Gd-SPIO-treated cancer cells. The use of counting beads during acquisition was avoided to evade the non-specific binding and aberrant side scatter of the cells. The acquisition of raw data for each sample was measured for 60 s. The total events collected for each sample depend on the treatment of cells due to reduced cell proliferation and death.

Estimation of cellular apoptosis

The later investigations were carried out by standard apoptosis assay pre- and post-exposure of Gd-SPIO nanoparticles to HepG2 cells in flow cytometry using Annexin-V and propidium iodide (PI) staining. Whereas, the cell membrane integrity or cell viability assay was further performed by the fluorescein di-acetate (FDA) assay using flow cytometry analysis. 10,000 events were collected for each sample which were analyzed using Cell Quest software (BD Biosciences) in FACS Calibre (Becton–Dickinson).

Reactive oxygen species (ROS) estimation

2′,7′-Dichlorofluorescin diacetate (DC-FDA) staining was performed to quantify the stress response in terms of reactive oxygen species (ROS) in cancer cells due to Gd-SPIO nanoparticle exposure. Flow cytometry was used to quantify the ROS levels pre- and post-Gd-SPIO nanoparticle exposure to HepG2 cells at different time points in culture. Briefly, 10 µM of DCFDA was added to HepG2 cells and incubated for 30 min in dark at 37 °C temperature. Unbound DC-FDA was washed twice with 1× PBS and resuspended in 500 µl volume of each sample for flow cytometry analysis. A total of 10,000 events were collected for each sample and analyzed using Cell Quest software (BD Biosciences).

Prussian blue staining

The labelling efficiency of Gd-SPIO nanoparticles was estimated using Prussian blue staining of HepG2 cells at different time points (10 min to 48 h) at different concentrations. The distribution of Gd-SPIO nanoparticles was estimated by identifying the iron staining and was documented using light microscope.

Cell labelling efficiency

The total iron content in HepG2 cells incubated with Gd-SPIO nanoparticles was quantified using total iron reagent set. In brief, cells labelled with potassium ferrocyanide in acidic condition were washed using culture medium followed by three times additional washing with 1× PBS. Further, cells were resuspended in 37% hydrochloric solution and incubated at 65–70 °C temperature for 30 min. The cell labeling efficiency was calculated by the retention of total iron content in the cell. The cell labeling efficiency of Gd-SPIO nanoparticles was estimated by preparing cell lysate of labeled samples at different time points using Iron Calorimetric Assay Kit (KA0814, Abnova) as per the manufacturer's instructions. For calculation of labeling efficiency standard curve was plotted before conducting the experiment. Following formula was used to calculate the labeling efficiency $C = \mathrm{Sa/Sv(nmol/\mu l}$, or mM),where Sa is the iron(II), iron(III), or total iron(II+III) content of unknown samples (in nmol) from standard curve. Sv is sample volume (µl) added into the assay wells.

Three individual experiments were performed to quantify the total iron contents and estimating the cell-labeling efficiency after incubating HepG2 cells with Gd-SPIO nanoparticles.

Expression studies

Total RNA was extracted using GITC method from pre- and post-treatment groups of HepG2 cells. Complementary DNA was prepared using OligodT primer. Whereas microRNAs were extracted from the control (non-treated) and Gd-SPIO-treated HepG2 cells after 48 h using miRNeasy mini kit (Qiagen, Valencia, CA, USA) according to the manufacturer's protocol. Universal stem loop primer was used to construct complementary DNA from extracted miRNAs. Three cancer-related genes [c-MET, TGF-β and hepatoma upregulated protein (hURP)] and two microRNAs (miRNA-199a and miRNA-181a) targeting various cancer pathways were quantified using specific primers. The primers sequences used to analyze the expression levels of specific mRNA transcripts and miRNAs are c-MET (F-CTTTGACGTGAAGTACGTGGT, R-CGTATGGCTACAAACACAGCAC), TGF-β (F-TCCATTGACGACGCCTTGG, R-CCC

TCTCTAACGTCTTGAGTCT), hURP (F-AAGCCTCGT TGAGTGGAAGG, R-AAGCAGGAACCCTCACAACC), GAPDH (F-CATGGGGAAGGTGAAGGTCGGA, R-TTG GCTCCCCCCTGCAAATGAG), miRNA-199a (F-AGG AAGCTTCTGGAGATCCTGC, R-TGCTCTCCCTTGCCC AGTCTAAC) and miRNA-181a (F-ACACTCCAGCTG GGAACATTCAACGCTGTCGG, R-CTCAACTGGTGT CGTGGA) and U6-miRNA (F-GCGCGTCGTGAAGCG TTC, R-GTGCAGGGTCCGAGGT). SYBR green-based quantitative real-time polymerase chain reaction (RT-qPCR) was performed to evaluate the changes in gene expression and miRNA expression levels pre and post-nanoparticles exposure. Relative fold values were calculated using $2^{-\Delta\Delta Ct}$ method (Livak and Schmittgen 2001).

Statistical analysis

All statistical analyses were performed using GraphPad Prism software (Version: V). One way and two way ANOVA was performed to identify the significance in single and multiple variants. Percentage cell viability was compared in different groups using formula: $A_{test}/A_{control} \times 100$. Inhibition rate of cells pre- and post-nanoparticle exposure was calculated using the optical densitometric analysis of each sample in triplicated in three different cohort studies using the formula: IR (%) = $1-OD_{test}/OD_{control} \times 100$. The percentage cell viability was calculated using formula: percentage viability = 100−IR (%). Glyceraldehyde 3-phosphate dehydrogenase (GAPDH) was used for the normalization of test samples during gene expression analysis whereas U6 miRNA was used as endogenous control for normalization of miRNA expression changes in test samples as compared to the controls. PCR efficiency of each transcript was calculated using $Y = mx + c$ formula. Each transcript was analyzed in triplicates in three different set of experiments. The mean was taken for each sample and the relative fold value of each transcript was calculated using the $2^{-\Delta\Delta CT}$ method by StepOne (Version 2.2) software in StepOne real-time PCR. All the results were expressed as mean ± SEM (standard error of mean). p value ≤ 0.05 was considered statistically significant for all the variables.

Results

Gd-SPIO nanoparticle synthesis and characterization

Hydrostatic chemical synthetic approach provided crystalline powder of Gd-SPIO nanoparticles with high purity at lower temperature. Schematic representation for the synthesis and major properties of Gd-SPIO nanoparticles is represented in Fig. 1a. FT-IR studies demonstrated stretching and bending vibrations of Gd-SPIO nanoparticles at 3750 and 1603.80/cm. The hydrostatic synthesis resulted in the formation of self-assembled nanostructure framework as demonstrated by thermal and XRD analysis. The vibration frequencies of Gd-SPIO nanoparticles do not change with the aging which represents that the quantum size of nanoparticles remains controlled thereby not altering the oxidation of metal ions. The average Gd-SPIO nanoparticle size was estimated to be approximately 41.65 nm as calculated by Debye–Scherer equation. SEM analysis of Gd-SPIO nanoparticles showed porous structures with different sizes due to aggregation (Fig. 1b). We found that changes in surface morphology of Gd-SPIO nanoparticles depend upon the reaction conditions and type of metal precursors used. UV–vis spectra of Gd-SPIO nanoparticles showed a strong peak at 700 nm representing highly pure nature of the nanoparticles (Fig. 1c).

Biocompatible nature of Gd-SPIO nanoparticles

The biocompatibility nature of Gd-SPIO nanoparticles was evaluated both in vitro, using human hepatocytes, and in vivo, using male Wister rats. SEM analysis of human hepatocytes with Gd-SPIO nanoparticle exposure for 72 h showed intact cellular morphology and extra-cellular matrix (ECM) (Fig. 1d). Percentage cell viability post-nanoparticle exposure for 72 h did not show significant variations with increasing the nanoparticle concentrations from 10 µg/ml to 1 mg/ml as compared to untreated cells (referred as control) (Fig. 1e). Histological analysis of vital organs of male Wister rats exposed to 1 mg/ml concentration of Gd-SPIO nanoparticles did not show any visible tissue manifestation or adverse pathologies (Fig. 1f). Other biological compatibility parameters for Gd-SPIO nanoparticles have been demonstrated in our earlier study (Athar et al. 2016).

Dual-MRI contrast properties

In vitro MRI of Gd-SPIO nanoparticles was performed using 1.5T clinical MRI machine at pH 7.4 to validate the potential of gadolinium (Gd) as T1 and super paramagnetic iron oxide nanoparticles as T2 MRI contrast agents residing in a single bi-metallic nanoparticle. MRI contrast imaging showed strong T1 MR signal with increasing the concentration of nanoparticles and represented the relaxivity coefficient of 14.3/mM/s (as obtained from the R1 relaxivity plots) due to strong interaction between the gadolinium and water molecules. The lower r2/r1 ratio (2.1) demonstrated highly enhanced T1 contrast of gadolinium ion (Fig. 2a). Furthermore the r2/r1 relaxation ratio was found to be enhanced (12.23) during T2-weighted MRI in nanoparticle-treated cells when compared with the control condition (untreated cells) (Fig. 2b).

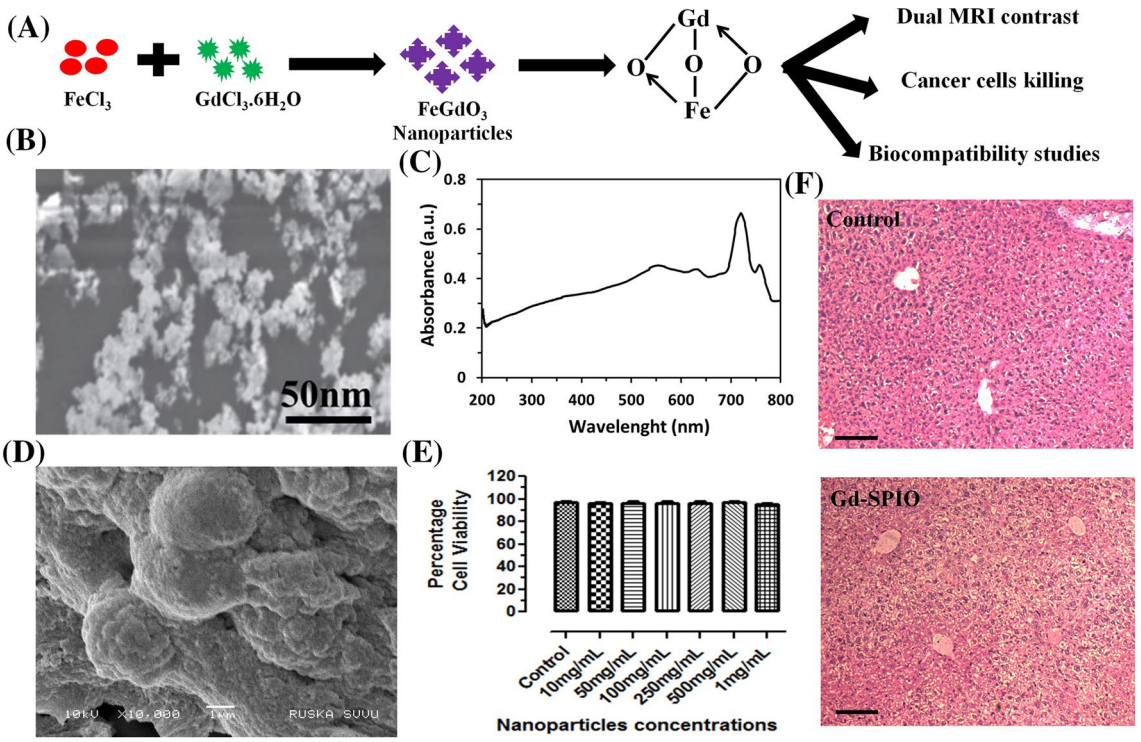

Fig. 1 **a** Schematic representation of Gd-SPIO nanoparticles ($FeGdO_3$) synthesis and inherent properties of MRI contrast, paramagnetism and biocompatibility. **b** SEM of synthesized Gd-SPIO nanoparticles showing < 50 nm size. **c** UV–vis spectra of Gd-SPIO nanoparticles after complete solubilization. **d** SEM image showing intact surface of human primary hepatocytes exposed to 1 mg/ml of Gd-SPIO nanoparticles for 72 h. **e** MTT cell viability assay showing no significant change in percentage cell survival of human primary hepatocytes exposed to different concentrations of Gd-SPIO nanoparticles for 72 h. **f** H&E staining of male Wister rat liver microsections of control (i.e. without nanoparticle injection) and Gd-SPIO- (1 mg/ml) treated group showing absence of any pathological feature (magnification: ×10, scale bar: 20 μm)

Nanoparticles uptake and SCA analysis

SCA analysis of HepG2 cells labeled with Gd-SPIO nanoparticles revealed significant increase in side scatter (SSC) of cells exposed with increasing the incubation time up to 120 min. No significant change in SSC was observed after 24 and 48 h of incubation when compared with the untreated cells (Control). This analysis revealed that nanoparticle uptake is highest at 120 min and almost removed or excreted from the cells after prolonged incubation time (24 and 48 h) (Fig. 3).

Changes in HepG2 cell viability post-nanoparticle exposure

The simultaneous analysis of cell viability along with the SCA revealed no significant change in cell viability up to 120 min whereas at 24 and 48 h the cancer cell viability was decreased up to 70 and 50%, respectively, in the presence of highest Gd-SPIO nanoparticle concentration (1 mg/ml) (Fig. 4a).

Changes in cellular apoptosis and ROS levels

The apoptosis assay revealed continuous increase in apoptosis rate of cells post-Gd-SPIO nanoparticle exposure with increasing the incubation time from 10 min to 48 h. The highest level of apoptosis was found after 48 h of exposure whereas the amount of necrotic cells remained constant (Fig. 4b). The ROS analysis did not show significant change for 120 min whereas it was increased drastically after 24 and 48 h of Gd-SPIO nanoparticle exposure Fig. 4c).

Cell-labeling efficiency and intracellular nanoparticle concentrations

Further to verify internalization and release of Gd-SPIO nanoparticles from the cancer cells, Prussian blue staining was performed which demonstrated highest level of internalization up to 120 min (Fig. 5a). With increasing the time duration most of the nanoparticles were found to be released at 24 and 48 h into the surrounding microenvironment. The cancer cell labeling efficiency increased with

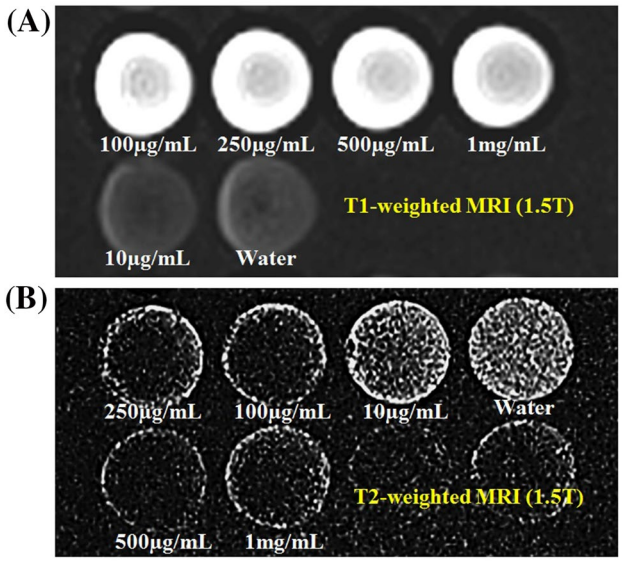

Fig. 2 **a** T1-weighted MRI image (obtained by 1.5T Magnetome) of cells incubated with different concentrations of Gd-SPIO nanoparticles showing highly enhanced contrast even at very low concentration up to 100 µg/ml. **b** T2-weighted MRI contrast of cells incubated with different concentrations of Gd-SPIO nanoparticles showing enhanced contrast with increasing the concentration

increasing the concentration of Gd-SPIO nanoparticles (Fig. 5b) which was quantified by the estimation of intracellular iron content (Fig. 5c, d). Whereas the total iron content in cells was significantly high at 500 µg/ml and 1 mg/ml concentrations when compared to others. More interestingly, the iron content was significantly reduced after 24 and 48 h of incubation.

Gene expression analysis

The gene expression analysis of liver cancer markers using RT-qPCR showed downregulation for oncogenic transcripts such as c-MET, TGF-β and hURP after Gd-SPIO nanoparticle exposure (1 mg/ml) for 48 h (Fig. 6a).

Micro-RNA expression analysis

Micro-RNA expression studies in HepG2 cells post-exposure to Gd-SPIO nanoparticles (1 mg/ml) showed upregulation of miRNA-199a (Fig. 6b) and miRNA-181a-7p (Fig. 6c) after 48 h.

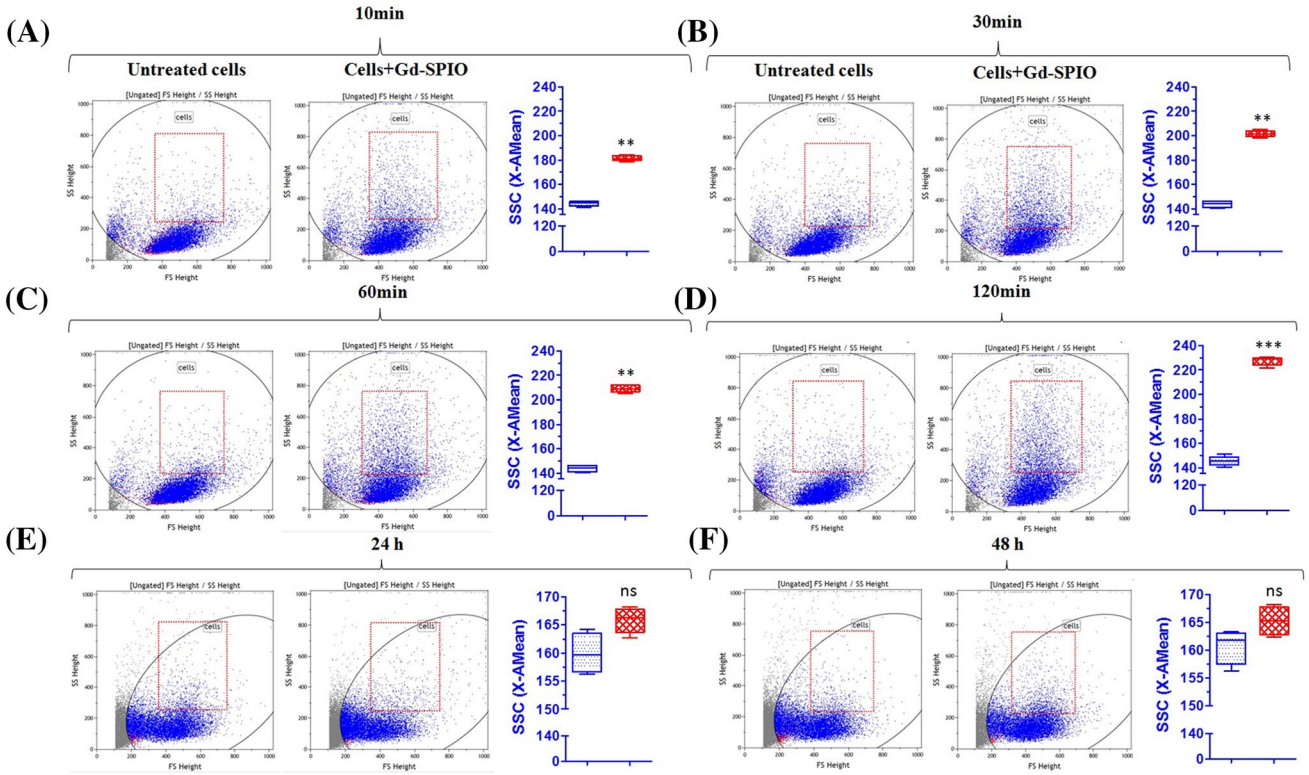

Fig. 3 **a**–**f** Side-scatter plots of flow cytometry-based analysis showing changes in HepG2 cancer cell granularity after in vitro exposure of Gd-SPIO nanoparticles (1 mg/ml) for different time points (Blue bar: untreated cells, Red bar: nanoparticles treated cells, $^{**}p < 0.001$, $^{***}p < 0.0001$, ns = non-significant, i.e. $p > 0.05$)

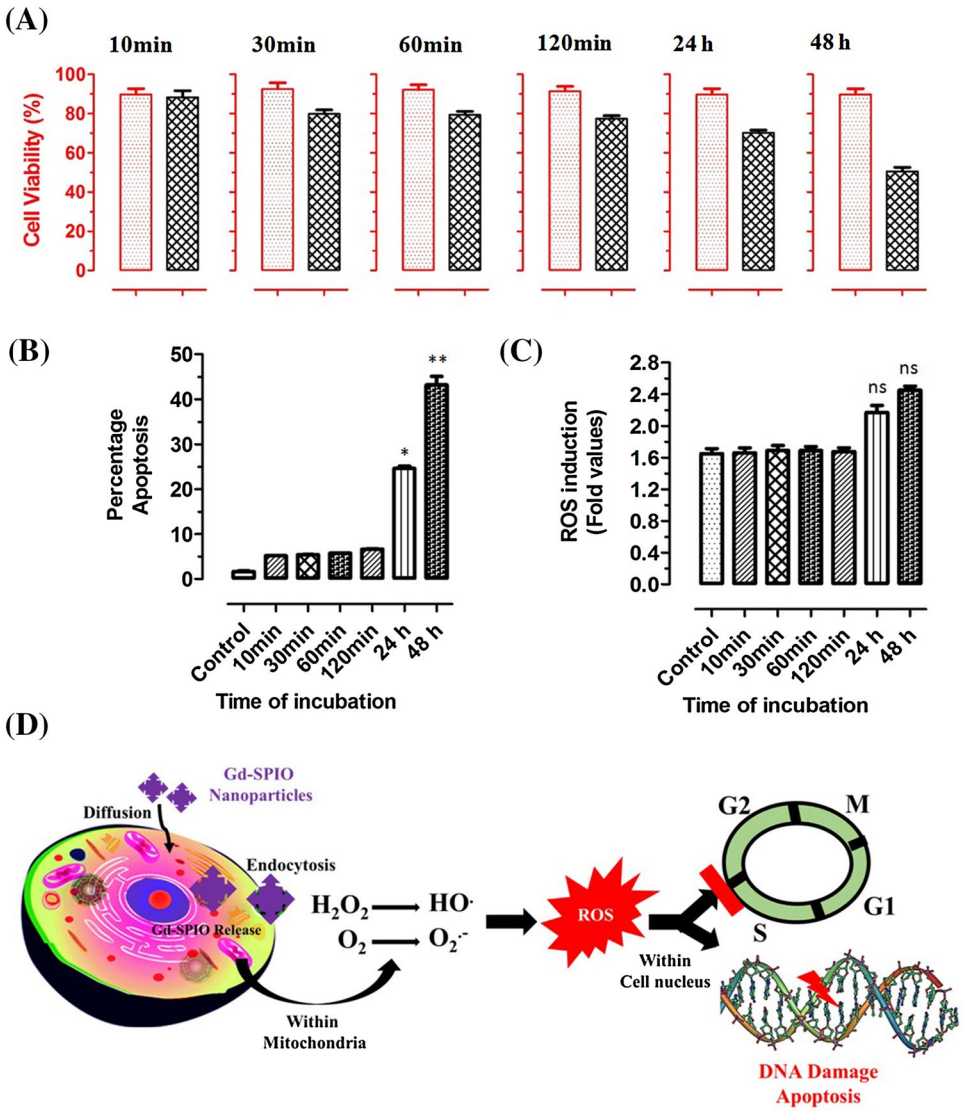

Fig. 4 Changes in **a** percentage HepG2 cell viability (estimated through FDA-based flow cytometry analysis). Red bar: untreated cells, Black bar: nanoparticle-treated cells. **b** Percentage cell apoptosis at different time points during exposure to Gd-SPIO nanoparticles (1 mg/mL). **c** ROS generation due to formation of free radicals in HepG2 cells and **d** predicted mechanism for cellular dynamics after Gd-SPIO nanoparticle exposure to HepG2 cells (*$p < 0.01$, **$p < 0.001$, ns = non-significant, i.e. $p > 0.05$)

Discussion

The present study explores the unique properties of bimetallic nanoparticle (Gd-SPIO) comprising gadolinium and iron ions. The results demonstrate that Gd-SPIO nanoparticles can be used for the effective killing of cancer cells without functionalization. The cost-effectiveness and hydrolytic synthesis approach offer the tuneable and ease of functionalization for enhanced contrast imaging and therapeutic possibilities (Athar et al. 2016). Additionally Gd-SPIO nanoparticles are less than 50 nm in size with dual MRI contrast which can be utilized for enhanced clinical imaging and real-time monitoring of drug targeting mechanisms. We also report a unique self-therapeutic property of Gd-SPIO nanoparticles in hepatoblastoma cells (HepG2) through real-time flow cytometry analysis. The schematic representation of the study outline has been depicted in Fig. 1a.

The flow cytometry-based SCA analysis represents cell size in forward scatter whereas cellular granularity in side scatters. The nanoparticle integration inside the cells was identified by SCA due to the light scattering nature of Gd-SPIO which can be easily detected by comparing with the untreated cells after surpassing the detection threshold. We observed significant increase in side scatter of cells exposed to Gd-SPIO nanoparticles with increasing the incubation time up to 120 min which later showed no significant change (after 24 and 48 h) in relation to the un-treated cells. This analysis revealed that nanoparticle uptake is highest at 120 min and released from the cells after 24 and 48 h (Fig. 2). These data were well supported by the findings demonstrated in Fig. 5b, d wherein cell labeling efficiency was found gradually increased with the time whereas the total iron content retained in cells was significantly less after 24 and 48 h of incubation when compared to 120 min. The complete removal of Gd-SPIO nanoparticles from HepG2

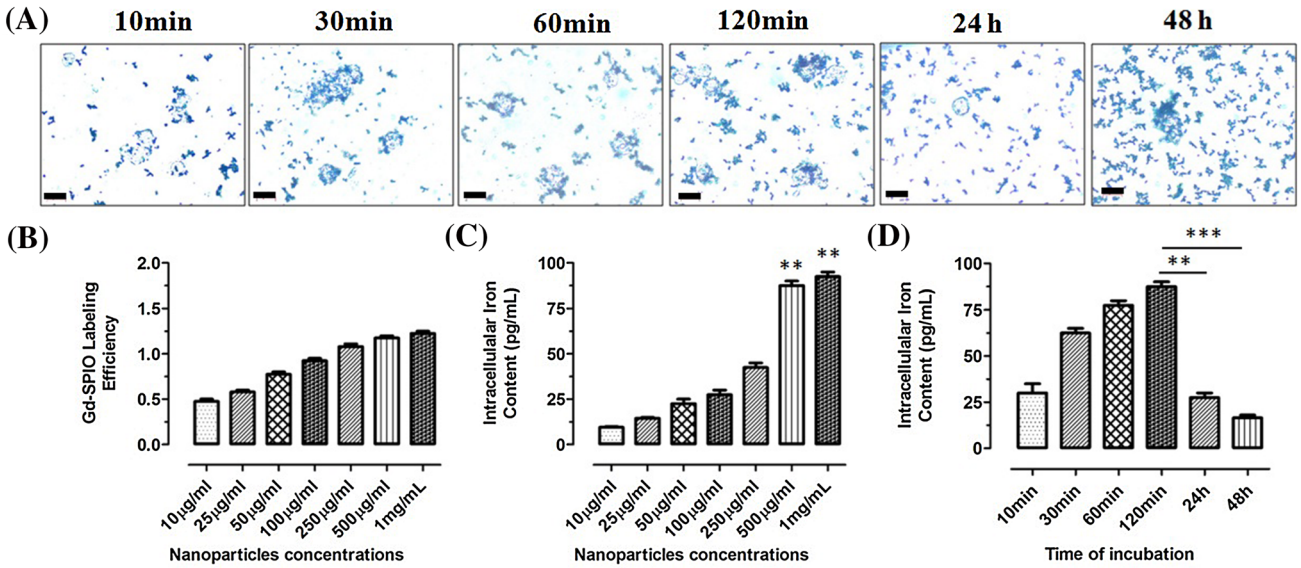

Fig. 5 **a** Prussian blue staining of Gd-SPIO nanoparticles in cell suspension at different time points in culture showing increased uptake up to 120 min and release from cells after 24 and 48 h post-exposure (scale bar: 20 µm, resolution: ×40). **b** The labelling efficiency of Gd-SPIO nanoparticles and **c** intracellular nanoparticle (measured in terms of iron content) concentration in HepG2 cells showed gradual increase with increasing the nanoparticle concentration. **d** The amount of nanoparticles inside the cells was highest after 120 min which was significantly reduced after 24 and 48 h (**$p < 0.001$, ***$p < 0.0001$)

cells can be due to exosomic transportation or apoptotic and necrotic cell death or cell membrane damage.

The simultaneous analysis of cell viability along with the SCA revealed no significant change in cell viability up to 120 min whereas at 24 and 48 h the cancer cell viability was decreased up to 70 and 50%, respectively, in the presence of highest Gd-SPIO nanoparticle concentration (1 mg/ml) (Fig. 3a). The apoptosis assay revealed continuous increase in apoptosis rate of cells with the increasing Gd-SPIO nanoparticle concentration whereas the amount of necrotic cells remained constant (Fig. 3b). The ROS analysis did not show significant change up to 120 min whereas it was increased drastically after 24 and 48 h of Gd-SPIO nanoparticle exposure in a dose-dependent manner (Fig. 3c). Collectively these quantitative flow cytometry-based analyses of Gd-SPIO nanoparticle uptake and their effect on HepG2 cells showed a unique panel for real-time assessment of nanoparticle interaction and internalization in cancer cells. The predictive mechanism for the anti-cancer effect of Gd-SPIO nanoparticles concluded that higher Gd-SPIO concentration exposure to HepG2 cells results in increased level of ROS production that results in cell cycle arrest and further leads to DNA damage and ultimately apoptotic cell death (Fig. 3d). These findings provide unique self-therapeutic anti-cancer property of Gd-SPIO nanoparticles. Further to verify these data, nanoparticle internalization and release from the cancer cells were identified using Prussian blue staining of nanoparticle exposed cells (Fig. 5a). The cancer cell labeling efficiency was increased with increasing the concentration of Gd-SPIO nanoparticles (Fig. 5b) which was identified by intracellular iron content estimation (Fig. 5c, d).

This particular strategy highlights the considerable capacity of SCA in combination with simultaneous detection of several other important parameters in flow-cytometry for Gd-SPIO nanoparticle applicability in highly personalized medicine for real-time quantification and self-therapeutic effect in cancer cells. Further expression analysis of mRNA as well as miRNA using RT-qPCR showed downregulation for cancer transcripts such as c-MET, TGF-β and hURP (Fig. 6a) and up regulation of miRNA-199a (Fig. 6b) and miRNA-181a-7p (Fig. 6c) after Gd-SPIO nanoparticle exposure for 48 h. Suh molecular aberrations in cancer cells along with enhanced ROS and apoptosis may lead to cancer cell death (Fig. 6d). The possible mechanism for this can be explained as the overexpression of c-MET mRNA is a prominent event in liver cancer which is triggered by cytokines like IL-6, TNF-α and TGF-β (Granito et al. 2015). In addition, the enhanced expression of c-MET allows increased binding of HGF proteins on it which stimulates several cancer pathways for enhanced cell growth, invasion and protection from apoptosis (Webb et al. 1998; Daveau et al. 2003; Sierra and Tsao 2011; Lee et al. 2013). Thus downregulation of c-MET and hURP protein important for cancer cell progression after Gd-SPIO nanoparticles exposure provide evidence for anti-cancer effect of these

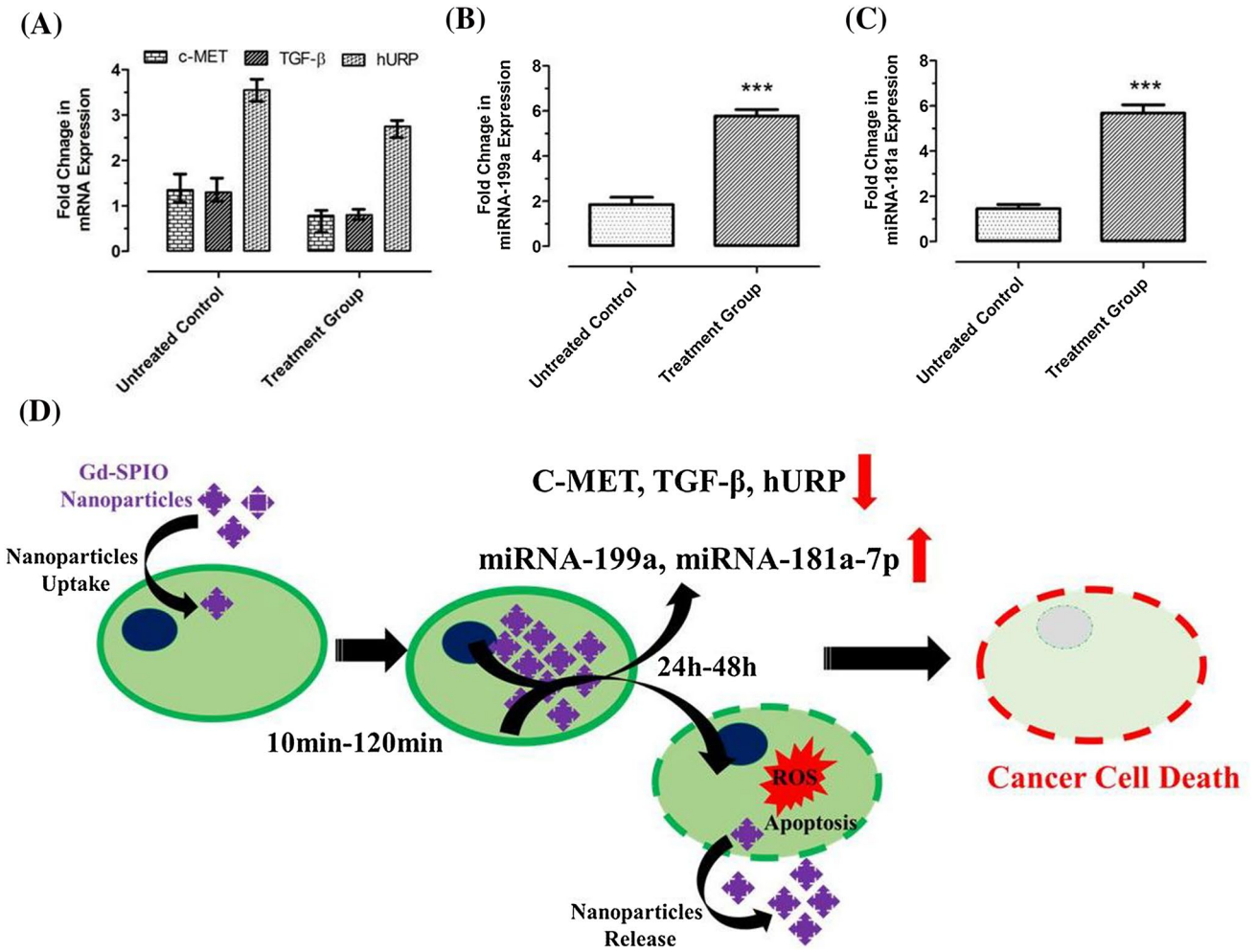

Fig. 6 Expression studies. **a** Fold change in the expression of cancer markers after 48 h of exposure of HepG2 cells with Gd-SPIO nanoparticles showing reduction as compared to untreated control groups. Whereas the expression levels of **b** miRNA-199a and **c** miRNA-181a-7p was significantly enhanced after nanoparticle exposure. **d** Schematic representation showing the overall effect of Gd-SPIO nanoparticle exposure to HepG2 cells. These cellular and molecular events lead to the activation of several toxic mechanisms within the cancer cells which further results in cancer cell death. ***$p = 0.0001$

nanoparticles. Another evidence was obtained from the expression levels of non-coding regulatory molecules such as miRNA-199a which is upregulated after Gd-SPIO nanoparticle exposure. MiRNA-199a downregulation in cancer cells is one of the common and quantitative events due to its direct binding with the c-MET receptor protein which leads to enhanced HGF binding on c-MET resulting in increased cancer cell proliferation and invasion (Fornari et al. 2010). Similarly, miRNA-181a-7p is also a direct target for c-MET whose downregulation in cancer cells leads to increased survival, invasion and morphogenesis (Korhan et al. 2014). The upregulation of miRNA-181a-7p expression after Gd-SPIO nanoparticle exposure to HepG2 cells provides additional evidence for its self-therapeutic property. Such molecular events may find its real applicability in normal malignant as well as drug-resistant cancer treatment after functionalization as described in our earlier studies (Khan et al. 2015; Vishwakarma et al. 2015, 2017).

Conclusion

The present study explores a multi-variant approach to monitor nanoparticle uptake and intracellular processing in real-time which could serve a unique platform for high-throughput screening of nanoparticle-based studies in cancer cells. This study demonstrated a unique strategy for real-time quantification of cellular uptake of Gd-SPIO nanoparticle-based SCA analysis using flow cytometry. We also observed self-therapeutic nature of non-functionalized Gd-SPIO nanoparticles which induces cancer cell death by production of reactive oxygen species and apoptotic events. Furthermore,

Gd-SPIO nanoparticles also enhance the expression levels of miRNA-199a and miRNA-181a-7p which results in decreased levels of cancer markers such as C-met, TGF-β and hURP. Conclusively, the real-time assessment of self-therapeutic properties of Gd-SPIO nanoparticles with the help of flow cytometry-based SCA analysis in combination with cellular and molecular approaches represents a unique multifaceted platform to explore potential of such nanoparticles in future applications.

Acknowledgements All authors thank CLRD, DCMS for providing the infrastructure and facility to perform experiment. SKV thanks Dr. Marshal Dhayal (IIT-BHU, Varanasi) for his support in generating UV–vis spectra of the nanoparticle.

Compliance with ethical standards

Conflict of interest None.

References

Arvizo RR, Bhattacharyya S, Kudgus RA, Giri K, Bhattacharya R, Mukherjee P (2012) Intrinsic therapeutic applications of noble metal nanoparticles: past, present and future. Chem Soc Rev 41:2943–2970

Arvizo RR, Saha S, Wang E, Robertson JD, Bhattacharya R, Mukherjee P (2013) Inhibition of tumor growth and metastasis by a self-therapeutic nanoparticle. Proc Natl Acad Sci USA 110:6700–6705

Athar T, Vishwakarma SK, Bardia A, Khan AA (2016) Super paramagnetic iron oxide and gadolinium (FeGdO3) nanopowder synthesized by hydrolytic approach passes high level of biocompatibility and MRI-based dual contrast property for competent molecular imaging and therapeutic interventions. Biomed Phys Eng Exp 6(2):025010

Benezra M, Penate-Medina O, Zanzonico PB, Schaer D, Ow H, Burns A, DeStanchina E, Longo V, Herz E, Iyer S, Wolchok J, Larson SM, Wiesner U, Bradbury MS (2011) Multimodal silica nanoparticles are effective cancer-targeted probes in a model of human melanoma. J Clin Invest 121(7):2768–2780

Bhattacharya R, Mukherjee P (2008) Biological properties of "naked" metal nanoparticles. Adv Drug Deliv Rev 60:1289–1306

Bridot JL, Faure AC, Laurent S, Riviere C, Billotey C, Hiba B, Janier M, Josserand V, Coll JL, Elst LV, Muller R, Roux S, Perriat P, Tillement O (2007) Hybrid gadolinium oxide nanoparticles: multimodal contrast agents for in vivo imaging. J Am Chem Soc 129(16):5076–5084

Chan MH, Lin HM (2015) Preparation and identification of multifunctional mesoporous silica nanoparticles for in vitro and in vivo dual-mode imaging, theranostics, and targeted tracking. Biomat 46:149–158

Daveau M, Scotte M, François A, Coulouarn C, Ros G, Tallet Y, Hiron M, Hellot MF, Salier JP (2003) Hepatocyte growth factor, transforming growth factor alpha, and their receptors as combined markers of prognosis in hepatocellular carcinoma. Mol Carcinogen 36:130–141

Fornari F, Milazzo M, Chieco P, Negrini M, Calin GA, Grazi GL, Pollutri D, Croce CM, Bolondi L, Gramantieri L (2010) MiR-199a-3p regulates mTOR and c-Met to influence the doxorubicin sensitivity of human hepatocarcinoma cells. Cancer Res 70:5184–5193

Granito A, Guidetti E, Gramantieri LJ (2015) c-MET receptor tyrosine kinase as a molecular target in advanced hepatocellular carcinoma. Hepatocell Carcin 2:29–38

Jiang W, Kim BY, Rutka JT, Chan WC (2008) Nanoparticle-mediated cellular response is size-dependent. Nat Nanotechnol 3:145–150

Khan AA, Vishwakarma SK, Bardia A, Paspala SAB, Athar T, Venkateshwarlu J, Abkari A, Murthy GSN (2015) Targeted homing of transplanted human neural precursor cells tagged with super paramagnetic iron oxide nanoparticles for the treatment of spinal cord injury. J J Regener Med 1:007

Korhan P, Erdal E, Atabey N (2014) MiR-181a-5p is downregulated in hepatocellular carcinoma and suppresses motility, invasion and branching-morphogenesis by directly targeting c-Met. Biochem Phys Res Commun 450:1304–1312

Krishnamurthy S, Gnanasammandhan MK, Xie C, Huang K, Cui MY, Chan JM (2016) Monocyte cell membrane-derived nanoghosts for targeted cancer therapy. Nanoscale 8:6981–6985

Lee SJ, Lee J, Sohn I, Mao M, Kai W, Park CK, Lim HY (2013) A survey of c-MET expression and amplification in 287 patients with hepatocellular carcinoma. Anticanc Res 33:5179–5186

Livak KJ, Schmittgen TD (2001) Analysis of relative gene expression data using real-time quantitative PCR and the 2(-Delta Delta C(T)) method. Methods 25(4):402–408

Mayhew TM, Muhlfeld C, Vanhecke D, Ochs M (2009) A review of recent methods for efficiently quantifying immunogold and other nanoparticles using TEM sections through cells, tissues and organs. Ann Anat 191:153–170

Rengan AK, Jagtap M, De A, Banerjee R, Srivsatva R (2014) Multifunctional gold coated thermo-sensitive liposomes for multimodal imaging and photo-thermal therapy of breast cancer cells. Nanoscale 6:916–923

Rengan AK, Bukhari AB, Pradhan A, Malhotra R, Banerjee R, Srivastava R, De A (2015) In vivo analysis of biodegradable liposome gold nanoparticles as efficient agents for photothermal therapy of cancer. Nano Lett 15:842–848

Sierra JR, Tsao MS (2011) c-MET as a potential therapeutic target and biomarker in cancer. Adv Med Onc 3:S21–S35

Vishwakarma SK, Paspala SAB, Bardia A, Khan AA (2015) Magnetic nanoparticle tagged stem cell transplantation in spinal cord injury: a promising approach for targeted homing of cells at the lesion site. Neurol Ind 63:460–461

Vishwakarma SK, Sharmila P, Bardia A, Chandrakala L, Raju N, Sravani G, Sastry BVS, Habeeb MA, Khan AA, Dhayal M (2017) Use of biocompatible sorafenib gold nanoconjugates for reversal of drug resistance in human hepatoblastoma cells. Sci Rep 7:8539

Webb CP, Taylor GA, Jeffers M, Fiscella M, Oskarsson M, Resau JH, Vande Woude GF (1998) Evidence for a role of Met-HGF/SF during Ras-mediated tumorigenesis/metastasis. Oncogen 17:2019–2025